Response to Referee 1

Dear referee

Please find enclosed the response to your comments.

On behalf of all authors,

Angela Limare

Referee's comments are italicized and addressed; manuscript text follows with changes tracked.

... a technical comment by Cochard was posted in the online discussion of this paper, and it seems to me that some of his comments should be addressed more explicitly than the authors did in their response.

Changes have been made to the text as explained in the response to Dr Cochard comment. In addition to that, a reference to the remarkable book of Ghilia and Pritt (1998) was added into the section 2.3. The software Light3D was better described as follows:

The algorithm we used was developed at the Laboratory of Solid State Mechanics of the University of Poitiers, France and is available as a commercial, software package called Light3D. The software allows the user to choose the number of phase-shifted projected patterns (3, 8, 16 or 32) and phase unwrapping can be performed with or without 8 gray code images. The encoded patterns are sent from the computer to a Sanyo PLV-Z5 video-projector. A black and white 1280 x 1024 pixels μeye Stemmer Imaging CCD camera was used for image acquisition. Since light beams are not parallel, the introduced phase shifting is not constant across the whole image. The algorithm implemented into the software recomputes the true phase shifts using Fast Fourier Transform (FFT). Therefore, the need to have a constant grid pitch over the entire image is also overcome. This requirement is essential when using the Fast Fourier Method as proposed by Takeda et al 1982 (section 2.2).

Inside of the rectangular image the object can be of any shape. The object mask is determined such as: if the intensity of the fringe pattern is the same, this indicates that it is an outside point so the mask is set to zero and is set to 255 for an inside point if

the intensities are different. The phase is obtained modulo 2π for each internal point (i.e. when mask = 255). Then the phase needs to be unwrapped, but because of the noise or discontinuities, a second mask step is applied, according to a modified Bone algorithm, (Bremand, 1994). This method adopts a "quality" measure to guide the unwrapping by calculating the second order partial derivatives of the phase map and comparing them to a threshold value to detect the discontinuities. A point of discontinuity is then set to zero. When the mask procedure is finished, the phase unwrapping algorithm can be applied. Each point having a mask value of 255 should give only one fringe number. If it is not the case a new threshold is applied until the discontinuity disappears.The image is scanned from one corner, the phase is unwrapped only if at least one of its 8 neighbours is treated. After the first pass, it is possible that several points could not be unwrapped. Then a second pass is performed from the opposite corner, and the cycle is repeated until all the points are analysed.

The phase-shifting technique of generating phase maps combined with the a quality based unwrapping makes this method suitable for the measurement of smooth objects with a very high resolution of measurement. When an extended height measuring range is required, the software can generate and use 8 gray code images. Gray coding provide a wide range, low resolution relief measurement method, but its combination with phase-shifting phase-map generation was proved to be very powerful when both extended measurement range and high resolution are required (Sansoni et al, 2000).

The method is based on a calibration procedure that uses a rotating plane at two positions separated by a given angle (Fig 1). The relief of the rotating plane is known in every point. The two phase fields obtained for the two positions of the plane are interpolated by a least square fit considering some (40) different lines distributed into the image according to the method given in Breque et al. 2000. The software allows the unwrapping of absolute phase maps as well as the unwrapping of the difference between two phase maps. The first type of calculation will produce a relief expressed with respect to the reference plane and the second one the relief deformation with respect to an initial state.

Can you be specific about what measurements you have obtained using this method that are different from previous measurements? In presenting your elevation data, what can you see that others haven't, and what will this allow you to do that others haven't?

Braiding has always been easy to reproduce in the lab and many experiments have been developped since the fifties (e.g. Ashmore, 1982; Federici and Paola, 2003; Schumm, 1977; Schumm et al., 1987). Yet the existence of multiple highly dynamic threads threads poses challenging issues. The technique we present here enables to address two key issues in braided river studies: topographic evolution of the bed and Shear stress distribution.

The novelty here is that we are able to get the instantaneous depth everywere on the braid plane. Thus for the first time we are able to compute PDFs of flow depth and probably shear stress distributions. To our knowledge there exist only two published PDFs for natural braided streams (Paola, 1996; Métivier et al., 2011) and one for experimental braided rivers (Tal and Paola, 2007). Both of these records are rough and limited precisely because of the acquisition techniques. Yet these studies and both theoretical and numerical consideration (e.g. Paola, 1996, 2001) clearly point to the key importance of such measurements in order to understand the physics of sediment transport in a braided river.

It seems to me that one thing you can do that others can't since you have high temporal resolution as well, is map dynamics. This is really the main point here - all the stuff in St. Anthony Falls Lab, for example (Jurassic Tank, Stream lab) uses a time of travel laser line. They have produced topographic maps that look at least as good as what you present in this paper - but what they do not have is the time resolution that you guys have. I think a representative difference map (a topo plot at time 1, a topo plot at time 2, and then a difference map using these two) figure would really help to show researchers the power of this approach. Rather than just saying that one can compute erosion rates, you can show a map of erosion/deposition rates and qualitatively point out "hot spots" of activity in braided river dynamics. This will get people really excited.

The suggested figure with topography plots at time 1, time 2, and the difference, was

added (Figure 9).

Figure 8: for part b, the plots are elevation profiles, NOT slope profiles (right?).

Yes, these are elevation profiles; the word change from slope to elevation has been made.

As for c, what is plotted is unclear. What are slope values at the edges of channels? How are channels chosen? Are these slopes measured in the downstream or cross-stream direction? How might they be useful?

Figure caption text has been modified to clarify the slope values histogram in 8c. The measurements are of cross-stream slopes just inside the edge of the channel (inner 3mm). Channels are isolated with the 3rd-quartile water depth threshold discussed in the text. Such measurements are useful for studying channel geometry and stability, and relating these to other measured properties, such as the local Shields stress.

In a separate set of microscale braided river experiments, the focus was on the dynamically evolving topography, and particularly on channel characteristics and dynamics (Reitz et al., in preparation). The study demonstrates how a moire method can be used to characterize a full range of statistics beyond just topography and depth. Calibration proceeded as above, with slightly different camera distances resulting in 0.93 mm/pixel resolution. Data was again collected via a series of 8 phase-shifted images, and deconstructed with Light3D software. Topography data for the measurements shown here were collected after the system had evolved from a flat bed to the dynamic equilibrium condition of equal input/output sediment flux, after one hour of steady water and sediment input. The 60 cm by 60 cm focus region of measurements was located in the downstream half of the system, to avoid potential inlet effects. The bulk relief values of this area are characterized in Fig. 7 a, generally within a range of 5mm incision and +2mm accretion. An initial scan with water running was followed by a scan taken two minutes after water flow had been stopped, and water depths were determined following the procedure outlined in Sect. 2.7 (Fig. 7b). Water depth values peak at a value of about 0.5 mm, and vary down to depths of 2 to 3 mm. In this study data was also collected on various aspects of the channels. In order to isolate

the channelized areas in a systematic manner, small, noisy water depth values were eliminated by setting a threshold on the water depth data set to only include depths up to the third statistical quartile of depth values (see Fig. 8a for a color-depth image of channelized water depths as isolated by this threshold). Having used this method to isolate the channels, channel characteristics such as number, width, length, and spacing were measured. The within-channel elevation profiles could also be tracked; see Fig. 8b for profiles of the five longest continuous threads of the study region, where it was possible to resolve sub-millimeter-scale features on the channel floors. Additionally, within-channel slopes at the banks were measured perpendicular to flow, as defined over a given distance inward of channel boundaries (Fig. 8c). Measurements such as these can inform our understanding of channel geometry organization, especially when combined with information about local Shields stress and bank migration rate, both of which can be extracted from a time-sequence of relief and water depth data. Finally, by differencing successive topographic scans (Fig. 9), we can produce a series of maps of erosional and depositional features as they evolve through time. With the high temporal resolution feasible with this method of measurement, we can gain new insight into the dynamic evolution of braided rivers.

References

Ashmore, P.: Laboratory modelling of gravel bed braided stream morphology, Earth. Surf. Process. Landforms, 7, 201–225, 1982.

Federici, B. and Paola, C.: Dynamics of channel bifurcations in noncohesive sediments, Water Resources Research, 39, 1162, 2003.

Métivier, F., Narteau, C., Lajeunesse, E., Devauchelle, O., Liu, Y., and Ye, B.: A new simple integral technique to analyze bedload transport data, in: River, Coastal and Estuarine Morphodynamics, IAHR (International Association of Hydraulic Engineering and Research), 2011.

Paola, C.: Incoherent Structure: Turbulence as a Metaphor for Stream Braiding, in: Coherent Flow Structures in Open Channels, 1996.

Paola, C.: Modelling stream braiding over a range of scales, Gravel Bed Rivers V, pp. 11–46, 2001.
Schumm, S. A.: The fluvial system, John Wiley & Sons Inc., 1977.
Schumm, S. A., Mosley, M. P., and Weaver, W. E.: Experimental Fluvial Geomorphology, John Wiley & Sons, Chichester, 1987.
Tal, M. and Paola, C.: Dynamic single-thread channels maintained by the interaction of flow and vegetation, Geology, 35, 347, 2007.
Ghilia, D. C. and Pritt, M. D..: Two-dimentional Phase Unwrapping: theory, algorithms, and software, Wiley Science, 1998.

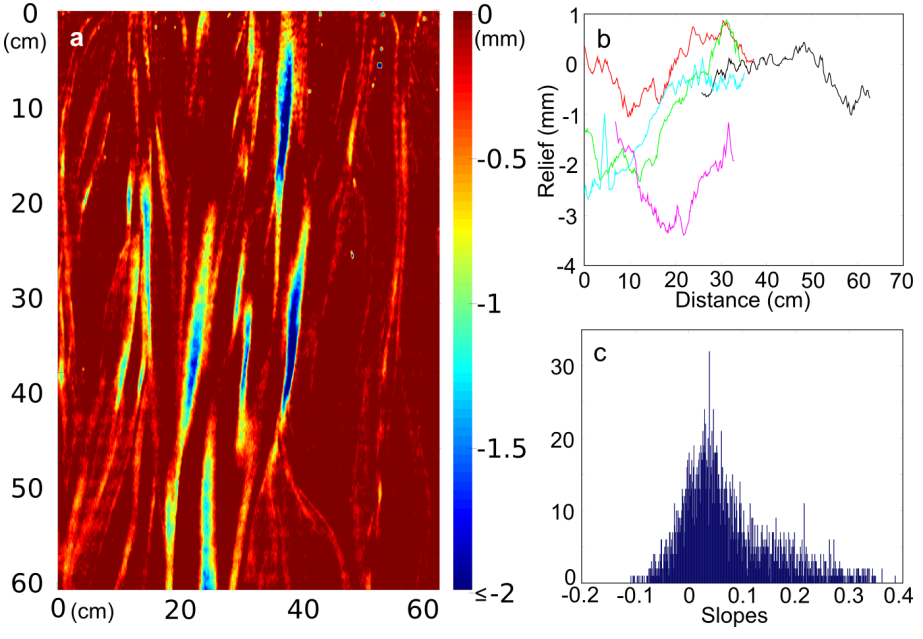

Fig. 8. (a)Planview of analyzed section of the braided river system. Colors correspond to water depth values. The direction of water flow is from the top to the bottom of the image; channelized threads are visible as vertical lines. (b) Within-channel elevation profiles of the five longest continuous channel threads. Profiles are plotted from an x-value corresponding to the distance down section (a) at which the channel begins. (c) Histogram of cross-stream slope values within the channels, at the channel banks (outer 3mm). Channel boundaries are defined using the wet fraction 3rd -quartile threshold discussed in the text.

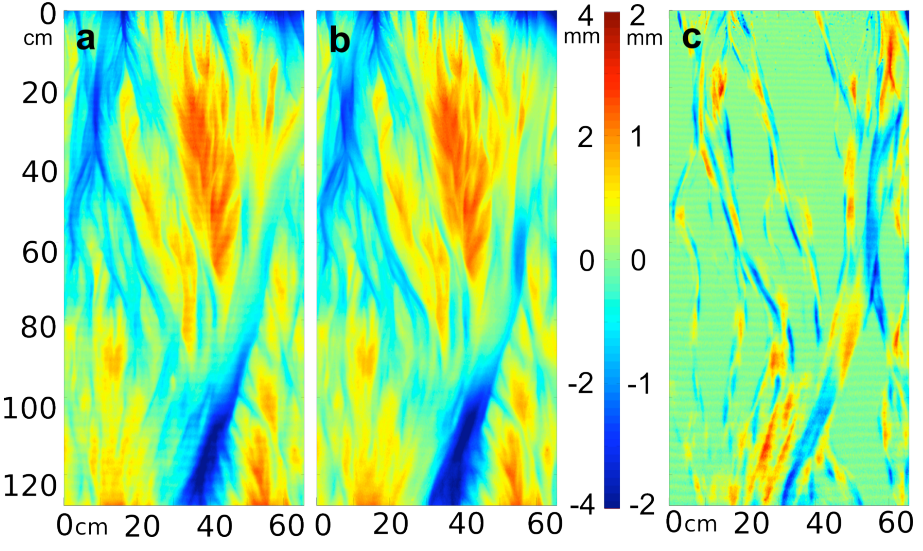

Fig. 9. (a) Topography scan of a developed braided river system, with flow direction from top to bottom of the image, and (b) scan repeated five minutes later. By subtracting the first scan from the second, we can produce (c) a map of the erosional and depositional features of the landscape.